

Dynamics of singularities in a constrained elastic plate

Arezki Boudaoud*, Pedro Patrício†, Yves Couder* & Martine Ben Amar*

* Laboratoire de Physique Statistique de l'ENS (associated with CNRS and the universities Paris VI and Paris VII), 24 rue Lhomond, F-75231 Paris Cedex 05, France

† Centro de Física da Matéria Condensada, Universidade de Lisboa Av. Prof. Gama Pinto 2, 1649-003 Lisbon, Portugal

Large deformations of thin elastic plates usually lead to the formation of singular structures which are either linear¹⁻⁴ (ridges) or pointlike⁵⁻⁸ (developable cones). These structures are thought to be generic for crumpled plates^{3,5}, although they have been investigated quantitatively only in simplified geometries^{1-4,6-8}. Previous studies⁹⁻¹¹ have also shown that a large number of singularities are generated by successive instabilities. Here we study, experimentally and numerically, a generic situation in which a plate is initially bent in one direction into a cylindrical arch, then deformed in the other direction by a load applied at its centre. This induces the generation of pairs of singularities; we study their position, their dynamics and the corresponding resistance of the plate to deformation. We solve numerically the equations describing large deformations of plates; developable cones are predicted, in quantitative agreement with the experiments. We use geometrical arguments to predict the observed patterns, assuming that the energy of the plate is given by the energy of the singularities.

In the absence of constraints, the two main curvatures κ_1 and κ_2 of a plane plate are zero. It is easy to bend the plate, that is, to give it a finite curvature in one direction so that it becomes cylindrical or conical. The curvature and thus the bending energy are then approximately evenly spread in the plate. It scales as $E_b \approx Eh^3$, E being the Young's modulus of the plate material and h its thickness. However, once bent in one direction, it is difficult to bend the plate also in the other direction because this will tend to create a finite Gauss curvature ($G = \kappa_1\kappa_2$) which can be only be acquired by stretching. The stretching energy is $E_s \approx EhR^2$, R being a typical length of the plate. As $E_s/E_b \approx (R/h)^2$ is large at small thickness, the deformation is pure bending almost everywhere and there is non-zero gaussian curvature only at singularities where the energetically expensive stretching is localized.

Here we study a plate initially curved in one direction (the x -direction), being clamped at two of its extremities (Fig. 1). The clamping provides two tunable parameters: the distance between the clamped sides d ; and the two equal angles (α) between the sheet and the horizontal direction at $x = \pm d/2$. The other two sides of the plates, at $y = \pm L/2$, are free. The plate is cylindrical (Fig. 1a). The cylinder axis is in the y -direction. A conical tip then pushes down the plate at its centre. The control parameter is the vertical displacement, Z , of the centre. This problem can be considered as the two-dimensional extension of the elastic arch investigated by Pippard^{12,13}. However, whereas the elastic arch has only bending deformations, the plate here may have stretching deformations as well.

Indeed, when the plate centre is displaced, two d-cones linked by an inverted ridge appear (Fig. 1a, e). As the vertical displacement of the centre Z is increased, the two d-cones move towards the clamped boundaries. The plate is still invariant by the x and y mirror symmetries. When the vertical displacement reaches about $Z = 10$ mm, a continuous transition occurs, breaking the two mirror symmetries. Two new d-cones appear, so that the four d-cones form a diamond which rotates about the centre (Fig. 1b, f). This rotation is either to the right or to the left. The plate is now

invariant by the 0-symmetry $(x, y) \rightarrow (-x, -y)$. At about $Z = 11.5$ mm a second continuous transition breaks all symmetries. The 4 d-cones move so that at $Z = 12$ mm they form a trapezoid (Fig. 1c, g). The trapezoid's larger edge is either to the left or to the right. The mirror symmetry $y \rightarrow -y$ is recovered. The trapezoid grows until two of its vertices reach the free sides of the sheet ($Z = 13$ mm). Then there is a discontinuous transition such that the plate becomes cylindrical (Fig. 1d). Note that these patterns are observed when the pushing tip is exactly at the centre of the plate (with a tolerance of about 0.1 mm). Once the adjustment is made, different realizations of the experiment (under the same conditions) show the two possible states following each continuous transition. The situation described here is the more general one: if the plate is long enough, all regimes are observed. If the length of the plate is decreased, first the trapezoid and then the diamond regime disappear: the d-cones reach the free boundaries and the discontinuous transition to a cylinder occurs earlier.

In elasticity theory, large deformation of plates are usually described by the Föppl von Kármán equations (FvK)¹⁴. These nonlinear equations are notoriously difficult, mainly because they

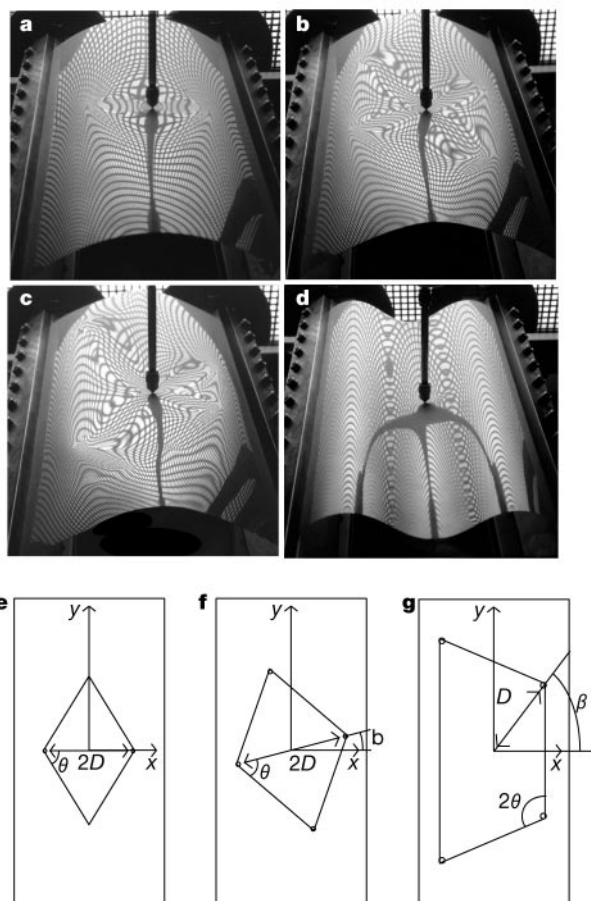


Figure 1 Observed patterns with a Mylar sheet of thickness $h = 0.35$ mm, Young's modulus $E = 3.8 \times 10^9$ N m⁻² and Poisson ratio $\nu = 0.4$. The aspect ratio is 2 (length $L = 35$ cm and width $W = 17.5$ cm). $\alpha = 20^\circ$ and $d = 16.5$ cm (see text for definitions). The results depend only slightly on the dimensions of the sheet. **a**, Vertical displacement of the centre $Z = 4$ mm: two d-cones located at $(x, y) = (\pm D, 0)$. **b**, $Z = 11.5$ mm: four d-cones forming a diamond at large rotation angle ($\beta \sim 30^\circ$). Two ridges link the d-cones. **c**, $Z = 12.5$ mm: 4 d-cones forming a trapezoid. **d**, $Z = 15$ mm: cylindrical shape. As Mylar has a large elastic limit there are no plastic (irreversible) deformations during this evolution. The experiment can thus be reproduced with the same sheet. **e-g**, Positions of the d-cones (black dots) in the **a**, **b** and **c**, respectively. The schemes give the definition of D , β and θ in the three regimes.

involve high-order derivatives and two types of deformations (stretching and bending) with energies of different orders of magnitude. A successful numerical procedure to overcome these difficulties has been proposed¹⁵. The plate is represented by finite elements and its energy is minimized. To obtain numerical convergence, the variables are changed by diagonalization of the energy hessian (re-conditioning) two or three times during the procedure.

Here, we compare experimental results and numerical solutions of the FvK equations. In Fig. 2, we show two numerical solutions and their energy as Z increases. Stretching is confined to the centre of the plate and to the d-cone tips. Bending dominates elsewhere. The pushing tip gives a spherical shape locally (non-zero Gauss curvature) to the plate so that there is stretching at the centre.

The experimental and the theoretical force versus displacement curve are represented in Fig. 3. The slope in zone II is larger than in zone I. This is explained by the numerics: some bending energy is localized near the boundaries. The agreement between numerics and experiment is good until zone III. So, we first concentrate on regimes I and II.

The contributions of the singularities dominate the energy of the plate. The energy of a ridge⁴ and the energy of a d-cone⁵⁻⁸ are given respectively by

$$E_r = F_r \kappa (R/h)^{1/3} \phi^{7/3} \quad (1)$$

$$E_d = F_d \kappa \ln(R/R_c) \phi^2 \quad (2)$$

Here $\kappa = Eh^3/12(1 - \nu^2)$ is the bending modulus, R the size of the singularity, ϕ its strength (the complement of the angle between the two sides of the ridge and the complement of the tip angle of the cone), $R_c = (\kappa/Eh)^{1/6} R^{2/3} \phi^{-1/3}$ is the radius of the core of the d-cone, $F_r \approx 1$ and $F_d \approx 100$ are shape factors. Under our conditions, where $h/R \approx 10^{-3}$ and $\phi \approx 0.1$, the energy of the ridges is negligible. As a consequence, the energy of the plate will be given by the energy of the d-cones.

Now we show that singularities are formed as soon as $Z \approx h$. We estimate the transition from the linear regime (the regime where the linearization of the FvK equations holds¹⁴) to the regime in which

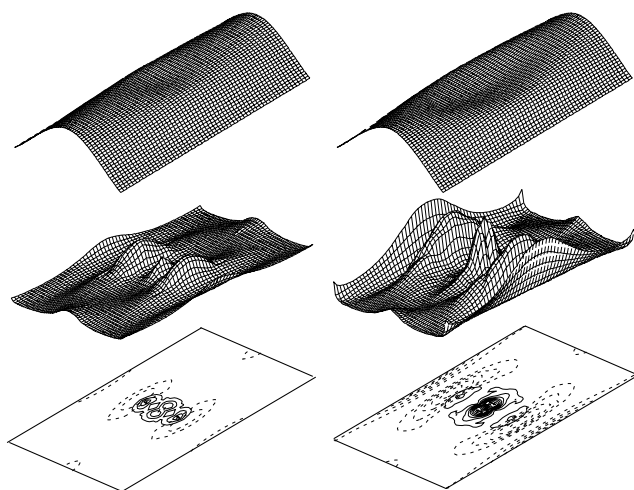


Figure 2 Two numerical situations with $\alpha = 20^\circ$ and $d = 16.5$ cm. Left, $Z = 5$ mm; right, $Z = 12$ mm. The procedure is a finite-element minimization of the plate energy, using reconditioning to obtain convergence. 471 minimization variables were used. Top, numerical configurations of the plate. Middle, energy density. A maximum at the centre (at the pushing tip) between two lateral maxima corresponding to two d-cones. For $Z = 12$ mm, some energy is localized at the clamped boundaries $(x, y) = (\pm d/2, 0)$. Bottom, contour lines of stretching energy (solid lines) and bending energy (dashed lines). The bending energy dominates except on very confined regions at the centre of the plate and the tips of the d-cones.

two d-cones appear. If $S = r^2$ is the area of the deformed zone, the strain and the curvature are given by $s \approx Z^2/r^2$ and $c \approx Z/r^2$. So the stretching and the bending energy scale as $E_s \approx Ehs^2S \approx EhZ^4/r^2$ and $E_b \approx Eh^3c^2S \approx Eh^3Z^2/r^2$ respectively. The comparison between these two expressions shows that the linear regime is only valid when $Z^2 < h^2$. The regime without singularities should correspond to the small region $Z \leq 0.35$ mm in Fig. 3.

In the two-d-cones regime, the central zone of the plate is diamond-shaped with two d-cones at the vertices where $y = 0$. The angular opening (Fig. 1e) of each d-cone (the angular opening of the inverted curvature zone) is always in the range $2\theta = 100-120^\circ$, the same as for a single d-cone^{7,8}. To find the positions of the d-cones, we use the following geometrical argument. Consider a section of the undeformed plate by the plane $y = 0$. Approximate it by its osculating parabola $z = kx^2$. When the centre is pushed, the arc $x \in (-D + \Delta, D - \Delta)$ of the parabola is transformed into the ridge of length $2D$ linking the two d-cones. The equality of the arc length and the ridge length yields $\Delta \approx 2/3k^3D^3$, so that

$$kD \approx \sqrt{kZ}(1 + 2/3kZ) \quad (3)$$

Here Z is the imposed vertical displacement. This equation is checked experimentally and numerically in Fig. 4, so that the geometrical description holds. In the x -section, the angle between the generatrices of a d-cone is $\psi \approx 2kD$. Now we must find the size R of the d-cone. Near its tip, the curvature due to the d-cone ψ/r is large (r is the distance to the tip). Far from the tip, the initial curvature of the plate $2k$ dominates. R is given by the matching $\psi/R \approx 2k$. Here the geometry gives all the characteristics of the d-cones; we only need to compute the energy from equation (2). If we use the solution found for the single d-cone⁶⁻⁸, $\phi = \psi/\mu$, $\mu = 4.8$ and $F_d = 67$. The solid line of Fig. 3 represents the force $F = dE_d/dZ$ calculated to the lowest order in kZ ($k = 5.7 \text{ m}^{-1}$). This description is only valid while the radius R of the d-cone is smaller than its distance to the boundary. This condition $D + R = W/2$ gives $Z_c = 10.9$ mm.

The rotation of the d-cones, leading to the diamond regime, can now be explained by a simple geometric argument. Consider the two d-cones with aperture angle 2θ and a section of the plate by the plane $y = \tan\beta x$ (Fig. 1g). When $Z = 0$, this section is approximated by $z = k \cos^2\beta s^2$, where s is the coordinate along the section. The geometrical results obtained for the 2 d-cones regime (equation

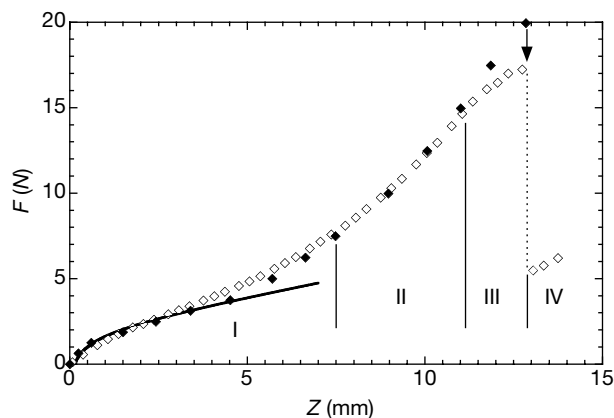


Figure 3 Force F versus displacement of the centre Z with $\alpha = 20^\circ$ and $d = 16.5$ cm. Force is measured with a piezoelectric cell allowing 10^{-2} N precision. Open diamonds, experimental result; filled diamonds, the numerics. The black arrow shows the numerical transition to regime IV. Solid line, theoretical prediction from equations (2) and (3), $F = 0.65 \ln(10.3Z)$. Regime I, two d-cones are observed. Regime II, almost linear, with a larger slope than in I. Regime III, the numerics overestimate the energy. Regime IV, cylindrical situation with no singularities.

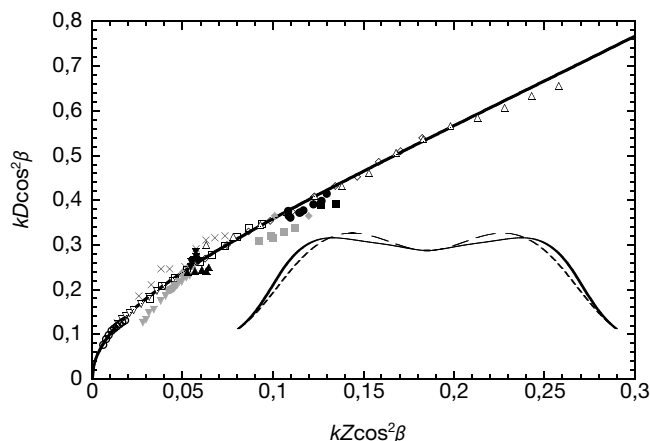


Figure 4 Distance between the dominant d-cones and the centre with various α and d values. k is half the mean curvature at the plate centre when $Z = 0$. Crosses, numerics; the other symbols are experimental. Open symbols, two-cones regime. Grey symbols, diamond regime. Black symbols, trapezoid regime. Solid line, theoretical prediction from equation (3). Inset curve ($Z = 6$ mm), \times cross-section of the plate (solid line); elastic arch (dashed line).

(3)) hold when k is replaced by $k \cos^2 \beta$ as is checked in Fig. 4. To lowest order in kZ , the d-cone radius is $R \approx D \approx \cos \beta \sqrt{Z/k}$. If the interaction between the d-cone and the clamped boundary is strong, the d-cone is constrained to move to a new position $\beta \neq 0$, in which the periphery of the d-cone (a circle of radius R) exactly touches the boundary of the plate, $D \cos \beta + R = W/2$. For Z near to Z_c , this condition leads to

$$\beta \approx \pm 4 \sqrt{2/3} kW \sqrt{k(Z - Z_c)} \quad (4)$$

Here $4\sqrt{2/3}kW = 3.3$ and $Z_c = 10.9$ mm compare well with the experimental $\beta = 3.1\sqrt{k(Z - Z_c)}$ with $Z_c = 10$ mm.

Now consider the second pair of d-cones. When their peripheries touch the clamped boundaries, $\beta + \theta \approx \pi/2$ so that $Z = Z_i \approx k(W/2 \sin \theta / (1 + \sin \theta))^2 = 15$ mm (with $\theta = 63^\circ$) which is comparable to the experimental $Z_i = 12$ mm. For $Z \geq Z_i$ all d-cones have to move along the clamped boundaries. If two of them are constrained to have an angular opening of 2θ , the only possible shape is a trapezoid. Compared to the two-d-cones regime, energy is gained in the diamond, and then the trapezoid regime. These configurations were not observed numerically, probably owing to the discretization. For this reason the numerics overestimates the force in region IV of Fig. 3. At $Z \geq 13$ mm the plate becomes cylindrical (pure bending deformations) so that the force jumps to a much smaller value (Fig. 3). This transition is well predicted by the numerics. The energy of the plate is then the same as the elastic arch¹³.

The experiment we have performed is typically a controlled version of what happens when a car is bumped. The difference is in the material; in metals the elastic limit is easily exceeded at the d-cones and then at the ridges. The first deformation of a plate is either cylindrical or conical. Most further deformations lead to the formation of pairs of d-cones and to the diamond-shaped deformation we have studied here. The observed shapes are determined by the geometry, and the energy of the plate can be computed using only the energy of the singularities. □

Received 22 February; accepted 24 July 2000.

1. Pogorelov, A. V. *Bendings of Surfaces and Stability of Shells*. (Translations of Mathematical Monographs No. 72, American Mathematical Society, 1988).
2. Witten, T. A. & Li, H. Asymptotic shapes of a fullerene ball. *Europhys. Lett.* **23**, 51–55 (1993).
3. Lobkovsky, A. E., Gentges, S., Li, H., Morse, D. & Witten, T. A. Scaling properties of stretching ridges in a crumpled elastic sheet. *Science* **270**, 1482–1485 (1995).
4. Lobkovsky, A. E. Boundary layer analysis of the ridge singularity in a thin plate. *Phys. Rev. E* **53**, 3750–3759 (1996).

5. Ben Amar, M. & Pomeau, Y. Crumpled paper. *Proc. R. Soc. Lond. A* **453**, 729–755 (1997).
6. Chaieb, S. & Melo, F. Experimental study of developable cones. *Phys. Rev. Lett.* **80**, 2354–2357 (1998).
7. Cerda, E. & Mahadevan, L. Conical surfaces and crescent singularities in crumpled sheets. *Phys. Rev. Lett.* **80**, 2358–2361 (1998).
8. Cerda, E., Chaieb, S., Melo, F. & Mahadevan, L. Conical dislocations in crumpling. *Nature* **401**, 46–49 (1999).
9. Chaieb, S. & Melo, F. Experimental study of crease formation in an axially compressed sheet. *Phys. Rev. E* **56**, 4736–4745 (1997).
10. Pomeau, Y. & Rica, S. Plaques très comprimées. *C.R. Acad. Sci. Paris* **325**, Série IIb, 181–187 (1997).
11. Pauchard, L. & Rica, S. Contact and compression of elastic spherical shells. *Phil. Mag.* **B78**, 225–233 (1998).
12. Pippard, A. B. The elastic arch and its modes of instability. *Eur. J. Phys.* **11**, 359–365 (1990).
13. Patricio, P., Adda-Bedia, M. & Ben Amar, M. An elastica problem: Instabilities of an elastic arch. *Physica D* **124**, 181–187 (1998).
14. Landau, L. D. & Lifshitz, E. M. *Theory of Elasticity* (Pergamon, Oxford, 1986).
15. Patricio, P. & Krauth, W. Numerical solutions of the Von Karman equations for a thin plate. *Int. J. Mod. Phys. C* **8**, 427–434 (1997).

Acknowledgements

We thank L. Quartier and M. Haddad for their valuable help. This work was finished during the stay of M.B.A. and A.B. at the Department of Mechanical Engineering of the MIT; M.B.A. and A.B. are grateful for the hospitality they received.

Correspondence and requests for materials should be addressed to A.B. (e-mail: arezki.boudaoud@lps.ens.fr).

Interconversion of single and double helices formed from synthetic molecular strands

Volker Berl*†, Ivan Huc‡*, Richard G. Khoury*, Michael J. Krische*§ & Jean-Marie Lehn*

* Laboratoire de Chimie Supramoléculaire, ISIS, Université Louis Pasteur, 4 rue Blaise Pascal, F-67000 Strasbourg, France

† Forschungszentrum Karlsruhe GmbH, Institut für Nanotechnologie, Postfach 3640, D-76021 Karlsruhe, Germany

‡ Institut Européen de Chimie et Biologie, ENSCPB, Av. Pey Berland, F-33402 Talence Cedex, France

Synthetic single-helical conformations are quite common, but the formation of double helices based on recognition between the two constituent strands is relatively rare. Known examples include duplex formation through base-pair-specific hydrogen bonding and stacking, as found in nucleic acids and their analogues, and polypeptides composed of amino acids with alternating L and D configurations^{1,2}. Some synthetic polymers³ and self-assembled fibres⁴ have double-helical winding induced by van der Waals interactions. A third mode of non-covalent interaction, coordination of organic ligands to metal ions^{5–7}, can give rise to double, triple and quadruple helices, although in this case the assembly is driven by the coordination geometry of the metal and the structure of the ligands, rather than by direct inter-strand complementarity. Here we describe a family of oligomeric molecules with bent conformations, which exhibit dynamic exchange between single and double molecular helices in solution, through spiral sliding of the synthetic oligomer strands. The bent conformations leading to the helical shape of the molecules result from intramolecular hydrogen bonding within 2'-pyridyl-2-pyridinecarboxamide units^{8–12}, with extensive intermolecular

§ Present address: University of Texas at Austin, Department of Chemistry and Biochemistry, Austin, Texas 78712, USA.